

# Spatiotemporal Augmentation on Selective Frequencies for Video Representation Learning

Jinhyung Kim<sup>1</sup>, Taeoh Kim<sup>2</sup>, Minho Shim<sup>2</sup>, Dongyoon Han<sup>3</sup>, Dongyoon Wee<sup>2</sup>,  
and Junmo Kim<sup>1</sup>

<sup>1</sup> School of Electrical Engineering, KAIST

<sup>2</sup> NAVER CLOVA Video

<sup>3</sup> NAVER AI Lab

**Abstract.** Recent self-supervised video representation learning methods focus on maximizing the similarity between multiple augmented views from the same video and largely rely on the quality of generated views. In this paper, we propose frequency augmentation (FreqAug), a spatio-temporal data augmentation method in the frequency domain for video representation learning. FreqAug stochastically removes undesirable information from the video by filtering out specific frequency components so that learned representation captures essential features of the video for various downstream tasks. Specifically, FreqAug pushes the model to focus more on dynamic features rather than static features in the video via dropping spatial or temporal low-frequency components. In other words, learning invariance between remaining frequency components results in high-frequency enhanced representation with less static bias. To verify the generality of the proposed method, we experiment with FreqAug on multiple self-supervised learning frameworks along with standard augmentations. Transferring the improved representation to five video action recognition and two temporal action localization downstream tasks shows consistent improvements over baselines.

**Keywords:** video representation learning, data augmentation, frequency

## 1 Introduction

There has been growing attention on transferring knowledge from large-scale unsupervised learning to various downstream tasks in natural language processing [12,62,44] and computer vision [8,21,18,5] communities. Considering data accessibility and possible applications, video representation learning has great potential as a tremendous amount of videos with diverse contents are created, shared, and consumed every day. In fact, unsupervised or self-supervised learning (SSL) of video via learning invariance between multimodal or multiple augmented views of an instance, including methods with or without negative samples, is being actively studied [19,1,56,45,23,7,52,43,16].

Recent studies in image SSL indicate a careful selection of data augmentation is crucial for the quality of the feature [54] or improving performance in

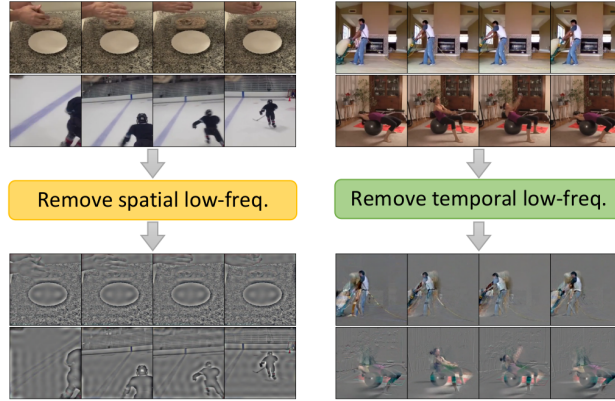


Fig. 1: **Impact of removing low-frequency components.** Filtering spatial low-frequency components (left) can attenuate spatially redundant information, *e.g.* surfaces without textures, while keeping the shape patterns. Removing temporal low-frequency components (right) filters out temporally stationary information, *e.g.* the background, while keeping the motion patterns.

downstream tasks [48, 63]. However, augmentations for video SSL have not been sufficiently explored yet. For videos, in terms of spatial dimension, the standard practice is adopting typical image augmentations in a temporally consistent way, *i.e.* applying the same augmentation to every frame in a video [43]. Meanwhile, a few previous works have investigated augmentations in the temporal dimension, including sampling a distant clip [16], sampling clips with different temporal scales [11] or playback speeds [7], and dropping certain frames [39]. Sampling-based augmentations in the temporal dimension, albeit effective, inevitably modulate a video as a whole regardless of signals in a clip varying at different rates. These methods are limited in resolving the spatial bias problem [32] of video datasets which requires distinguishing motion-related features from static objects or scenes. Adding a static frame [52] is a simple heuristic to attenuate the temporally stationary signal, but it is hard to generalize to the real-world’s non-stationary signal in both spatial and temporal dimensions. The need for a more general way to re-arrange and selectively process a video signal depending on the spatial and temporal changing rates motivates us to consider frequency domain analysis.

In digital signal processing, converting a signal to the frequency domain using discrete Fourier transform (DFT), then processing the signal is widely used in many applications. Filtering in the frequency domain is one example that attenuates a specific frequency range to remove undesirable components, such as noise, from the signal. With its effectiveness in mind, we propose filtering video signals in the frequency domain to discard unnecessary information while keeping desired features for the SSL model to learn.

Fig. 1 shows the outcome of filtering out low-frequency components from videos. When the spatial filter is applied, plain surfaces of objects in the scene are diminished while their boundary or shapes are maintained. As for the temporal filter, stationary parts of the video, *e.g.* static objects or the background, are removed while dynamic parts, *e.g.* a person moving, are retained. These results are aligned with the previous discoveries that high-frequency components carry essential information for image and video understanding [50,27].

In this work, we propose frequency augmentation (FreqAug), a novel spatio-temporal augmentation in the frequency domain by randomly applying a filter to remove certain frequency bands from the video. Specifically, we aim to alleviate representation bias for better transferability by filtering out spatially and temporally static components from the video signal. FreqAug is composed of a 2D spatial filter and a 1D temporal filter. The frequency band of each filter can be determined by the filter type and its cutoff frequency. In video SSL, FreqAug can be applied to each view independently on top of other video augmentations so that learned representation captures invariance between remaining frequency components. In particular, applying FreqAug with high-pass filter results in obtaining the representation with less static bias via focusing more on invariance between the instance and its high-frequency components. Note that what we are claiming is not that only the high-frequency components are important, but rather a matter of relative importance. Since FreqAug is applied randomly, low-frequency components still get involved in the invariance learning.

We demonstrate the effectiveness of the proposed method by presenting transfer learning performance on five action recognition datasets: both coarse-grained (UCF101 [47], HMDB51 [30]) and fine-grained (Diving48 [32], Gym99 [46], Something-Something-v2 [17]) datasets. Downstream action recognition performances are measured via either finetuning or low-shot learning evaluation protocol. Additionally, the learned features are evaluated via the temporal action segmentation task on Breakfast dataset [29] and the action localization task on THUMOS'14 dataset [24]. Empirical results show that FreqAug enhances the performance of multiple SSL frameworks and backbones, which implies the learned representation has significantly improved transferability.

## 2 Related Work

### 2.1 Video Self-supervised Learning

Unsupervised or self-supervised learning (SSL) through multi-view invariance learning has been widely studied for image recognition and other downstream tasks [55,8,21,9,18,5,10]. In video SSL, previous works exploited the view invariance based approaches from the image domain and explored ways to utilize unique characteristics of the video including additional modalities, *e.g.* optical flow, audio, and text [51,23,56,19,36,1,2,45]. However, we focus more on the RGB-based video SSL methods in this study. CVRL [43] proposed temporally consistent spatial augmentation and temporal sampling strategy, which samples two positive clips more likely from near time. RSPNet [7] combined relative speed

perception and video instance discrimination tasks for learning both motion and appearance features from video. Empirical results in [16] show four image-based SSL frameworks [9,18,8,5] can be generalized well to the video domain. They also presented a temporal persistency objective among multiple positive clips from a video. MoCo-BE [52] introduced a regularization that reduces background influences on SSL by adding a static frame to the video. Our work is also a study on data augmentation for video SSL, but propose to modulate the video signal in the frequency domain.

## 2.2 Frequency Domain Augmentations

Lately, several studies on frequency domain augmentation have been proposed for the 1D speech and 2D image domain. For speech or acoustic signal, a few works incorporated augmentations that are masking [40] or filtering [37] a spectrogram or mixing that of two samples [26]. In the image domain, Xu *et al.* [60] tackled the domain generalization problem by mixing spectrum amplitude of two images. A concurrent work [38] introduced randomly masking a certain angle of Fourier spectrum based on the spectrum intensity distribution for X-ray image classification. These methods are relevant to ours in that they randomly alter a spectrum for data augmentation. To the best of our knowledge, our method is the first 3D spatio-temporal augmentation in the frequency domain by filtering a certain frequency band selectively for video representation learning and we investigate the transferability to various downstream tasks.

## 3 Method

### 3.1 Preliminary

In this work, we aim to augment spatio-temporal video signals in a frequency domain by filtering particular frequency components. Discrete Fourier transform (DFT), a widely used technique in many digital signal processing applications, provides appropriate means of converting a finite discrete signal into the frequency domain for computers. For simplicity, let us consider 1D discrete signal  $x[n]$  of length  $N$ , then 1D DFT is defined as,

$$X[k] = \sum_{n=0}^{N-1} x[n] e^{-j(2\pi/N)kn}, \quad (1)$$

where  $X[k]$  is the spectrum of  $x[n]$  at frequency  $k = 0, 1, \dots, N-1$ . Since DFT is a linear transformation, the original signal can be reconstructed by inverse discrete Fourier transform (iDFT):

$$x[n] = \frac{1}{N} \sum_{k=0}^{N-1} X[k] e^{j(2\pi/N)kn}. \quad (2)$$



1D-DFT can be extended to the multidimensional DFT by simply calculating a series of 1D-DFT along each dimension. One can express d-dimensional DFT in a concise vector notation as,

$$X_{\mathbf{k}} = \sum_{\mathbf{n}=0}^{\mathbf{N}-1} x_{\mathbf{n}} e^{-j2\pi \mathbf{k}(\mathbf{n}/\mathbf{N})}, \quad (3)$$

where  $\mathbf{k} = (k_1, k_2, \dots, k_d)$  and  $\mathbf{n} = (n_1, n_2, \dots, n_d)$  are d-dimensional indices from  $\mathbf{0}$  to  $\mathbf{N} = (N_1, N_2, \dots, N_d)$  and  $\mathbf{n}/\mathbf{N}$  is defined as  $(n_1/N_1, n_2/N_2, \dots, n_d/N_d)$ . We omit the equation of d-dimensional iDFT as it is a straightforward modification from Eq. (2).

### 3.2 Filtering Augmentation in Frequency Domain

Filtering in signal processing often denotes a process of suppressing certain frequency bands of a signal. Filtering in frequency domain can be described as an element-wise multiplication  $\odot$  between a filter  $F$  and a spectrum  $X$  as,

$$\hat{X} = F \odot X, \quad (4)$$

where  $\hat{X}$  is a filtered spectrum. A filter can be classified based on the frequency band that the filter passes or rejects: low-pass filter (LPF), high-pass filter (HPF), band-pass filter, band-reject filter, and so on. LPF passes a low-frequency band while it filters out high-frequency components from the signal; HPF works oppositely. Let us consider a simple 1D binary filter, also known as an ideal filter, then LPF and HPF can be defined as,

$$F_{lpf}[k] = \begin{cases} 1 & \text{if } |k| < f_{co} \\ 0 & \text{otherwise,} \end{cases} \quad (5)$$

$$F_{hpf}[k] = 1 - F_{lpf}[k], \quad (6)$$

where  $f_{co}$  is the cutoff frequency which controls the frequency band of the filter.

In this work, we propose frequency augmentation (FreqAug, Fig. 2), which utilizes 3D-DFT with the binary filter approach to augment video data in the frequency domain by stochastically removing certain frequency components. Since video signals have three dimensions, *i.e.* T, H, and W, the filter also can be 3D and have three independent cutoff frequencies. We introduce a single spatial cutoff frequency  $f_{co}^s$  that handles both H and W dimension, and one temporal cutoff frequency  $f_{co}^t$  for T dimension. Then 1D temporal filters are identical to Eq. (5) and Eq. (6), and 2D spatial LPF can be defined as,

$$F_{lpf}^s[k_h, k_w] = \begin{cases} 1 & \text{if } |k_h| < f_{co}^s \text{ and } |k_w| < f_{co}^s \\ 0 & \text{otherwise,} \end{cases} \quad (7)$$

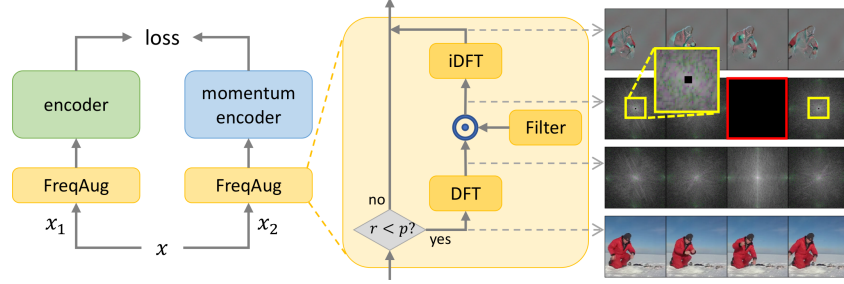


Fig. 2: **Frequency augmentation (FreqAug)**. Filtering in the frequency domain is a sequential process of 1) transforming a video to a spectrum by DFT; 2) applying the desired filter by element-wise multiplication; 3) transforming the filtered spectrum back to the video domain by iDFT. Video frames and their spectrum on the right are an example of applying spatio-temporal high-pass filters. In filtered spectrum (2nd row), low-frequency components of spatial (small black regions inside yellow boxes, see the first one for the close-up) and temporal (the red box) axis are removed. FreqAug is placed after other augmentations and randomly applied when  $r \sim U(0, 1)$  is less than the augmentation probability  $p$ .

and  $F_{hpf}^s$  is obtained in the same way as Eq. (6). Finally, the spatio-temporal filter  $\mathbf{F}$  can be obtained by outer product between the temporal filter  $F^t$  and the spatial filter  $F^s$  as,

$$\mathbf{F} = F^{st}[k_t, k_h, k_w] = F^t[k_t] \otimes F^s[k_h, k_w], \quad (8)$$

where  $\otimes$  is outer product. The final 3D filtered spectrum  $\hat{\mathbf{X}}$  can be represented as an element-wise multiplication between  $\mathbf{F}$  and the spectrum  $\mathbf{X}$  as Eq. (4).

Additionally, FreqAug has one more hyperparameter, the augmentation probability  $p$ , which determines how frequently the augmentation is applied. FreqAug processes the input only when the random scalar  $r$ , sampled from uniform distribution  $U(0, 1)$ , is less than  $p$ .

Fig. 2 presents a block diagram of FreqAug in MoCo [21] framework and visualization of a video sample and its spectrum at each stage of FreqAug. Note that FreqAug blocks operate with independent  $r$  for each view. For the spectrum, lower spatial frequencies are located near the center of the spectrum at each column ( $(k_h, k_w) = (0, 0)$ ) and lower temporal frequencies are located near the third spectrum ( $k_t = 0$ ). For visualization, we apply spatial and temporal HPF with  $f_{co}^s = 0.01$  and  $f_{co}^t = 0.1$  respectively. In the filtered spectrum (2nd row), spatial low-frequency (small black region inside yellow boxes) and temporal low-frequency (red box) components are removed.

## 4 Experiment

### 4.1 Datasets and Implementation Details

**Pretrain Datasets.** For pretraining the model, we use Kinetics-400 (K400) [6] and Mini-Kinetics (MK200) [57]. K400 is a large-scale video action recognition dataset with 400 classes and MK200 is a balanced subset of K400 with 200 classes. With the limited resources, K400 is too large for extensive experiments, so we choose MK200 as a major testbed to verify our method’s effectiveness. We also report results on K400 for comparison to previous models.

**Downstream Tasks.** For evaluation of the pretrained models, we use five different action recognition datasets: UCF101 [47], HMDB51 [30], Diving48 [32], Gym99 [46], and Something-something-v2 (SSv2) [17]. Following the standard practice, we report the accuracy of the finetuned model on the three datasets: UCF101, HMDB51, and Diving48. Note that we present split-1 accuracy for UCF101 and HMDB51 by default unless otherwise specified. For Gym99 and SSv2, we evaluate the models on the low-shot learning protocol using only 10% of training data. Finetuning on those datasets may dilute the effect of pretraining since they are relatively large-scale (especially the number of samples in SSv2 is about twice larger than that of our main testbed MK200). Nevertheless, evaluating models on those datasets is still meaningful because it reflects the impact of pretraining on a substantially different target domain. Furthermore, low-shot learning can simulate practical scenarios, where only a few labels are available for the target task. For temporal action localization downstream tasks, Breakfast [29] and THUMOS’14 [24] dataset are used.

**Self-supervised Pretraining.** For self-supervised pretraining, all the models are trained with SGD for 200 epochs. In terms of spatial augmentation, augmentations described in [9] are applied in a temporally consistent manner as our baseline. For temporal augmentation, randomly sampled clips from different timestamps compose the positive instances. Also, two clips are constrained to be sampled within a range of 1 second from each clip’s center frame. Each clip consists of  $T$  frames sampled from  $T \times \tau$  consecutive frames with the stride  $\tau$ .

In terms of FreqAug, we use the following two default settings in the experiments: 1) FreqAug-T (temporal) uses temporal HPF with cutoff frequency 0.1; 2) FreqAug-ST (spatio-temporal) is a combination of spatial HPF with cutoff frequency 0.01 alongside with FreqAug-T.

**Finetuning and Low-shot Learning.** We train the models for 200 epochs with the initial learning rate 0.025 without warm-up and zeroed weight decay for supervised finetuning and low-shot learning. Only fundamental spatial augmentations [16] are used for finetuning and low-shot learning.

**Temporal Action Localization.** We evaluate the learned representation on two temporal action localization tasks: action segmentation that allocates every frame into pre-defined action class and action localization that localizes class-specific temporal action snippets from backgrounds. We train an action segmentation model, MS-TCN [14] following the work [4], on Breakfast dataset [29]

Table 1: **Evaluation results of SlowOnly-50 model pretrained on Mini-Kinetics.** We demonstrate FreqAug with MoCo, BYOL, and SimSiam. Relative increments over the baseline augmentation are stated in the parenthesis. Low-shot denotes finetuning with only 10% of total training samples.

Method	Augmentation	Finetune			Low-shot	
		UCF101	HMDB51	Diving48	Gym99-10%	SSv2-10%
MoCo [9]	Baseline	87.0	56.5	67.8	29.9	25.3
	+ FreqAug-ST	90.0 (+3.0)	61.6 (+5.1)	71.0 (+3.2)	34.8 (+4.9)	28.1 (+2.8)
	+ FreqAug-T	89.8 (+2.8)	60.8 (+4.3)	70.3 (+2.5)	35.2 (+5.3)	28.1 (+2.8)
BYOL [18]	Baseline	88.4	59.8	70.3	38.7	29.5
	+ FreqAug-ST	90.5 (+2.1)	63.2 (+3.4)	72.4 (+2.1)	40.7 (+2.0)	31.2 (+1.7)
	+ FreqAug-T	90.5 (+2.1)	62.7 (+2.9)	72.5 (+2.2)	40.8 (+2.1)	31.6 (+2.1)
SimSiam [10]	Baseline	86.1	57.5	67.4	33.2	27.5
	+ FreqAug-ST	87.3 (+1.2)	57.3 (-0.2)	70.7 (+3.3)	33.7 (+0.5)	28.6 (+1.1)
	+ FreqAug-T	86.0 (-0.1)	58.6 (+1.1)	70.4 (+3.0)	34.1 (+0.9)	29.0 (+1.5)

with fixed features from the pretrained encoder. For temporal action localization model, we train a localization model, G-TAD [59] on THUMOS’14 [24] dataset. **Evaluation.** For Kinetics, UCF101, and HMDB51, we report average accuracy over 30-crops, *i.e.* temporally 10-crops and spatially 3-crops, following [15]. In the case of Diving48, Gym99, and SSv2, we report the spatial 3-crop accuracy with segment-based temporal sampling. For temporal action segmentation, frame-wise accuracy, edit distance, and F1 score at overlapping thresholds 10%, 25%, and 50% are used as evaluation. For temporal action localization, we measure mean average precision (mAP) with intersection-over-union (IoU) from 0.3 to 0.7.

**Backbone.** Our default encoder backbone is SlowOnly-50 (SO-50) which is a variant of 3D Residual Network (ResNet) originated from the slow branch of SlowFast network [15]. We evaluate our method on 3D-ResNet-18 (R-18) [20], R(2+1)D [49] and S3D-G [57] models as well.

**SSL Methods.** We implement MoCo [9], BYOL [18], and SimSiam [10] for the video model. We pretrain MoCo with batch sizes of 128 and 256 for MK200 and K400 training, respectively. For both BYOL and SimSiam, the batch size is set to 64 for training and synchronized BN [8] is used in the models. Please refer to Appendix for more implementation details.

## 4.2 Action Recognition Evaluation Results

In Table 1, we present evaluation results of three SSL methods with FreqAug pretrained on MK200. MoCo pretrained SO-50 with FreqAug-ST and FreqAug-T significantly improve the baseline in all five downstream tasks. The absolute increments of top-1 accuracy range from 2.5% to 5.3% depending on the task. We observe that FreqAug-ST shows comparable or better accuracy than FreqAug-T in four out of five tasks, indicating the synergy between spatial and temporal filter. Leveraging FreqAug to BYOL also shows improved performance over

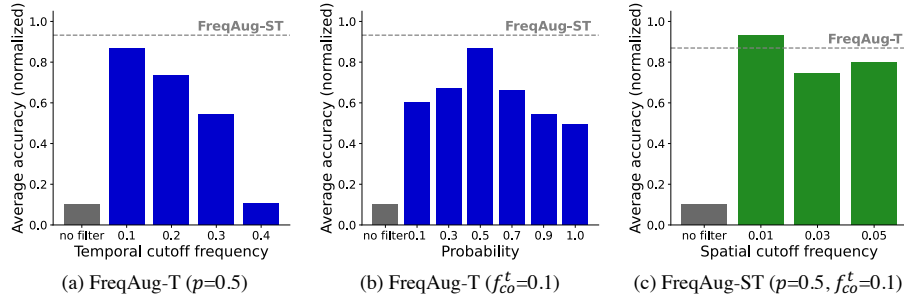


Fig. 3: **FreqAug hyperparameter ablations on Mini-Kinetics.** Three parameters are searched: (a) temporal cutoff frequency ( $f_{co}^t$ ) and (b) augmentation probability ( $p$ ) for FreqAug-T and (c) spatial cutoff frequency ( $f_{co}^s$ ) for FreqAug-ST. Other parameters set fixed with the value in the parenthesis. MoCo-pretrained SlowOnly-50 are used as a backbone for finetuning and low-shot tasks. Min-max normalized accuracies of 5 tasks are averaged.

the baseline augmentation on all downstream tasks. The absolute increments of BYOL (1.7% to 3.4%) are a bit less than those of MoCo because BYOL has a stronger baseline. The overall accuracy of FreqAug-ST and FreqAug-T in BYOL are similar, which is not observed in MoCo; this implies that differences between MoCo and BYOL, such as loss or existence of predictor MLP, may cause a different impact of FreqAug to learning dynamics. We also demonstrate FreqAug on SimSiam which has no momentum encoder, unlike the previous two methods. Note that we set  $p = 0.1$  and  $f_{co}^t = 0.2$  for FreqAug-ST for SimSiam. FreqAug with SimSiam enhances the accuracy on most downstream tasks, but the overall increase is a bit less than the numbers of other methods. We observe the marginally decreased numbers either on UCF101 or HMDB51; we speculate that the lack of the momentum encoder in SimSiam incurs the accuracy degradation. One possible explanation is that the momentum encoder in MoCo and BYOL contributes to stabilizing the invariance learning with relatively hard augmentation like FreqAug. The negative impact of hard augmentations on SimSiam is recently studied in literature [3]. Nonetheless, FreqAug is effective across SSL frameworks. These improvements are mostly achieved with a fixed hyperparameter setting searched for MoCo. Thus, better results are expected if SSL framework specific hyperparameters are searched for BYOL and SimSiam.

### 4.3 Ablation Study

**On Hyperparameters.** We conduct three types of ablation studies on MK200 in order to search proper hyperparameters ( $f_{co}^s$ ,  $f_{co}^t$  and  $p$ ) in Fig. 3. SO-50 pre-trained with MoCo is used as the baseline model. For ease of visualization, we first min-max normalize top-1 accuracies for each task using all ablation models, then present average accuracy over five action recognition tasks. We also mark

Table 2: **Backbone comparison on Mini-Kinetics.** We extensively evaluate FreqAug with diverse backbones, including SlowOnly-50 (SO-50), SlowOnly-18 (SO-18), 3D-ResNet-18 (R-18), R(2+1)D and S3D-G as the baselines for fine-tuning and low-shot learning tasks. Here,  $T$ : number of frames,  $\tau$ : input stride,  $H \times W$ : spatial resolution. Input resolutions are for the downstream task.

Backbone	$T \times \tau$	$H \times W$	Augmentation	Finetune			Low-shot	
				UCF101	HMDB51	Diving48	Gym99-10%	SSv2-10%
SO-50	$8 \times 8$	$128 \times 128$	Baseline	82.2	53.9	64.2	30.8	25.4
			+ FreqAug-ST	85.4 (+3.2)	58.6 (+4.7)	67.3 (+3.1)	33.7 (+2.9)	29.1 (+3.7)
			+ FreqAug-T	86.0 (+3.8)	58.0 (+4.1)	65.9 (+1.7)	34.3 (+3.5)	28.6 (+3.2)
SO-18	$8 \times 8$	$224 \times 224$	Baseline	82.4	51.9	65.0	26.9	21.6
			+ FreqAug-ST	86.7 (+4.3)	55.6 (+3.7)	67.1 (+2.1)	31.0 (+4.1)	24.1 (+2.5)
			+ FreqAug-T	85.7 (+3.3)	57.1 (+5.2)	68.4 (+3.4)	29.4 (+2.5)	23.9 (+2.3)
SO-18	$16 \times 4$	$224 \times 224$	Baseline	84.5	55.2	74.9	30.3	23.9
			+ FreqAug-ST	88.5 (+4.0)	57.8 (+2.6)	75.8 (+0.9)	35.3 (+5.0)	25.7 (+1.8)
			+ FreqAug-T	88.7 (+4.2)	58.8 (+3.6)	75.7 (+0.8)	34.7 (+4.4)	26.1 (+2.2)
R-18	$16 \times 2$	$224 \times 224$	Baseline	82.6	49.5	36.6	28.0	18.9
			+ FreqAug-ST	86.8 (+4.2)	56.9 (+7.4)	41.0 (+4.4)	32.8 (+4.8)	20.9 (+2.0)
			+ FreqAug-T	86.4 (+3.8)	55.9 (+6.4)	39.1 (+2.5)	32.3 (+4.3)	20.8 (+1.9)
R(2+1)D	$32 \times 2$	$128 \times 128$	Baseline	86.2	60.4	64.6	42.5	29.2
			+ FreqAug-ST	90.0 (+3.8)	65.9 (+5.5)	67.7 (+3.1)	48.4 (+5.9)	31.5 (+2.3)
			+ FreqAug-T	89.5 (+3.3)	65.2 (+4.8)	70.2 (+5.6)	48.3 (+5.8)	30.5 (+1.3)
S3D-G	$32 \times 2$	$224 \times 224$	Baseline	89.0	59.5	70.1	42.1	30.5
			+ FreqAug-ST	90.2 (+1.2)	63.6 (+4.1)	71.0 (+0.9)	44.5 (+2.4)	31.1 (+0.6)
			+ FreqAug-T	90.4 (+1.4)	62.2 (+2.7)	68.8 (-1.3)	44.3 (+2.2)	31.5 (+1.0)

the accuracy of models with default FreqAug-ST or FreqAug-T in dotted line for a better comparison. Note that the cutoff frequencies are searched in consideration of the minimum interval between each component:  $1/T$  for temporal and  $1/H$  (or  $1/W$ ) for spatial dimension.

First, we search four cutoff frequencies  $f_{co}^t \in \{0.1, 0.2, 0.3, 0.4\}$  for temporal HPF with augmentation probability  $p = 0.5$  in Fig. 3 (a). First three cases show improved downstream performance compared to the baseline (“no filter” in the figure), with notable improvement. Because  $f_{co}^t = 0.1$  is dominant than others on average, we set it as a default. If  $f_{co}^t$  becomes larger, then the performance increment over the baseline becomes smaller since too much information is removed. Second,  $p$  of FreqAug-T is searched in a range of  $[0.0, 1.0]$  while keeping  $f_{co}^t$  fixed to 0.1 in Fig. 3 (b). We found that the overall downstream performance is the best when  $p = 0.5$  which is the default setting of FreqAug-T. In addition, FreqAug-T enhances the performance regardless of  $p$ ; even in the case  $p = 1.0$  where temporal HPF is always applied. Lastly, we examine FreqAug-ST by adding spatial HPF on top of FreqAug-T with default hyperparameters found above. The spatial cutoff frequencies  $f_{co}^s \in \{0.01, 0.03, 0.05\}$  are tested in Fig. 3 (c). We observed that FreqAug-ST with  $f_{co}^s = 0.01$  improves the performance even more than FreqAug-T while a larger  $f_{co}^s$  has a negative impact on the performance. More ablation studies can be found in Appendix.

**On Diverse Backbones.** In Table 2, we validate FreqAug with five different backbones: SlowOnly-50 (SO-50), SlowOnly-18 (SO-18), 3D-ResNet-18 (R-18),

Table 3: **Comparison with RGB-based models pretrained on Kinetics-400.** Backbone, number of frames (T), and pretraining epochs are specified and all spatial resolutions are  $224 \times 224$ . The UCF101 and HMDB51 accuracies are averaged over 3 splits. Models highlighted in gray are pretrained with larger epochs. †: evaluated on split-1; ‡: ambiguous or not specified which splits are used; §: some modification from the original model.

Model	Backbone	T	Epochs	Finetune		
				UCF101	HMDB51	Diving48
RSPNet [7]‡	S3D-G	64	200	89.9	59.6	N/A
MoCo-BE [52]	I3D	16	50	86.8	55.4	62.4
ASCNet [22] †	S3D-G	64	200	90.8	60.5	N/A
$\rho$ MoCo ( $\rho = 2$ ) [16]†	SO-50	8	200	91.0	N/A	N/A
CVRL [43]	SO-50§	32	800	92.2	66.7	N/A
RSPNet [7]‡	S3D-G	64	1000	93.7	64.7	N/A
MoCo (ours)	SO-50	8	200	90.6	62.8	72.9
MoCo + FreqAug-ST	SO-50	8	200	92.1	65.6	74.0
MoCo + FreqAug-T	SO-50	8	200	91.8	65.1	73.8

R(2+1)D and S3D-G, which have various input resolutions (number of frames  $T$ , input stride  $\tau$ , spatial resolution  $H \times W$ ), depth, and network architecture. The detailed setup for each backbone is described as follows: 1) SO-50 with a low spatial resolution of  $128 \times 128$  trained with a larger batch size of 256, 2) SO-18 chosen for testing a shallow model with plain residual blocks (not bottleneck blocks) and two different temporal resolutions ( $8 \times 8$ ,  $16 \times 4$ ), 3) R-18 which has residual blocks with full 3D convolutions and its input clip has 16 frames with stride 2, 4) R(2+1)D which has factorized 3D residual blocks, and 5) S3D-G which has inception-style 3D blocks. Note that we pretrain R(2+1)D and S3D-G with the input temporal resolution  $16 \times 4$  and then finetune with  $32 \times 2$ . The results in Table 2 show FreqAug boost the performance in all cases regardless of spital and temporal input resolutions and the network architecture except finetuning S3D-G+FreqAug-T on Diving48. However, in the other 4 datasets, S3D-G with FreqAug surpasses the baseline model.

#### 4.4 Comparison with Previous Models

In Table 3, we present K400 experiments with FreqAug comparing to previous video SSL works. We report the average accuracy of 3 splits for UCF101 and HMDB51 following the standard practice [43,52,16]. We choose the SSL methods in Table 3 that allow for a fair comparison based on three criteria: multi-view invariance based, RGB-only (without multimodality including optical flow), and spatial resolution of  $224 \times 224$ . Note that  $\rho$  of the models from [16] indicates the number of views from different timestamps, so models with  $\rho = 2$  are directly comparable to our models. First of all, both FreqAug-ST and FreqAug-T



Table 4: **Temporal action segmentation on Breakfast.** All features are evaluated with MS-TCN model [14]. ‘Edit’ denotes edit distance. †: scores are averaged over 10 evaluations on split-1.

Method	Data	Acc.	Edit	F1@{0.10, 0.25, 0.50}		
SO-50 sup.† [13]	K400	59.0	59.5	54.7	49.2	37.6
LSFD, N [4]	K400	60.6	60.0	52.0	42.8	35.3
MoCo†	MK200	54.8	56.3	51.5	46.2	35.0
+ FreqAug-ST†		64.1	63.1	60.3	55.2	43.4
+ FreqAug-T†		62.5	61.9	58.1	52.8	41.0
MoCo†	K400	59.9	60.4	57.2	52.0	40.2
+ FreqAug-ST†		65.2	63.9	61.7	56.6	45.2
+ FreqAug-T†		<b>65.9</b>	<b>64.8</b>	<b>62.5</b>	<b>57.1</b>	<b>45.3</b>

Table 5: **Temporal action localization on THUMOS’14.** Features are pre-trained on K400 and evaluated with G-TAD [59]. †: scores are mean over 5 runs.

Method	Pretrain	mAP@0.3	mAP@0.4	mAP@0.5	mAP@0.6	mAP@0.7	Avg
TSM [58]	Sup.	46.6	39.5	30.1	20.1	12.2	29.7
TSM + BSP [58]		52.3	46.3	39.8	<b>30.8</b>	<b>21.1</b>	38.1
TSN†	Sup.	45.7	36.8	28.2	19.0	11.3	28.2
SO-50†		51.1	44.2	34.2	24.7	15.3	33.9
MoCo†	Self-sup.	52.2	45.6	37.3	28.0	18.2	36.3
+ FreqAug-ST†		54.1	47.4	39.4	29.6	19.8	38.1
+ FreqAug-T†		<b>55.4</b>	<b>48.7</b>	<b>40.3</b>	30.3	20.2	<b>39.0</b>

consistently outperform the baseline MoCo on UCF101, HMDB51, and Div-ing48. Compared with other models trained with similar epochs, MoCo with FreqAug outperforms all the others with similar training epochs. Interestingly, FreqAug demonstrates its training efficiency by defeating RSPNet on HMDB51 and approaching CVRL on UCF101; they are pretrained for 1000 and 800 epochs respectively. We expect training with more powerful SSL methods and longer epochs may be complementary to our approach.

#### 4.5 Other Downstream Evaluation Results

In Table 4, we report the results of temporal action segmentation task on the Breakfast dataset [29]. We experiment with the features extracted from MoCo pretrained SO-50 on MK200 and K400. In addition, we report the performance of the extracted feature by officially released SO-50 [13] pretrained on K400 by supervised learning. The results show that MoCo-pretrained with FreqAug substantially improves the baseline on all metrics. We conjecture that foreground motion can easily be separated in the videos with static backgrounds by the FreqAug-enhanced feature. Surprisingly, the features from MoCo with FreqAug pretrained on MK200 outperform the supervised K400-pretrained features. Fur-

Table 6: **Supervised pretraining with FreqAug.** SlowOnly-50 pretrained on MK200. Sup. denotes supervised action recognition accuracy.

Method	Sup.	Finetune			Low-shot	
	MK200	UCF101	HMDB51	Diving48	Gym99-10%	SSv2-10%
SlowOnly-50	77.4	91.0	61.0	72.3	36.4	25.5
+ FreqAug-ST	78.6	91.3	62.9	73.2	39.2	27.1
+ FreqAug-T	78.0	91.5	65.4	71.0	40.0	26.2

thermore, MoCo with FreqAug pretrained on K400 surpasses LSFD [4] in all metrics, which is the only video SSL method evaluated on this task.

In Table 5, we report the results of temporal action localization on THU-MOS’14 dataset [24]. We use the features extracted from MoCo pretrained SO-50 on K400. The results shows that MoCo features outperforms supervised features from RGB-only TSN [53] (two-stream model is used in original G-TAD [59]) and SO-50. Moreover, adding FreqAug to MoCo pretraining improves the localization performance even further compared to the baseline. We also compare our results to BSP [58], a localization-specific pre-training method and show similar or better localization performances. Note that BSP [58] is trained with TSM [33] backbone in supervised manners while ours are trained with fully unsupervised.

## 5 Discussion

### 5.1 FreqAug for Supervised Learning

One may wonder whether using FreqAug in supervised learning is still effective; here, we evaluate FreqAug in a supervised scenario to demonstrate the versatility of our method. Table 6 shows the performance of MK200 pretrained SlowOnly-50 by supervised learning for 250 epochs. Note that  $p=0.3$  is used since we observed lower accuracy with a too large  $p$ . When we applied FreqAug on top of basic augmentation, we observe overall performance improvements including the performance of the five downstream tasks and the MK200 pretraining task.

### 5.2 Analysis on Effect of FreqAug

In this subsection, we take a closer look at how the downstream performance of the features learned through FreqAug can be improved compared to the baseline. Fig. 4 shows t-SNE [35] plots of features from original clips (blue) with both high-frequency components (HFC) and low-frequency components (LFC) and either high-pass or loss-pass filtered clips (red) in spatial (a) and temporal (b) dimension; the distance between two features are measured using mean squared error (MSE). We compare features from MoCo pretrained SlowOnly-50 on MK200 with or without FreqAug-ST. The samples are from validation set of MK200 and  $f_{co}^s = 0.02$  and  $f_{co}^t = 0.2$  are set for both HPF and LPF. We

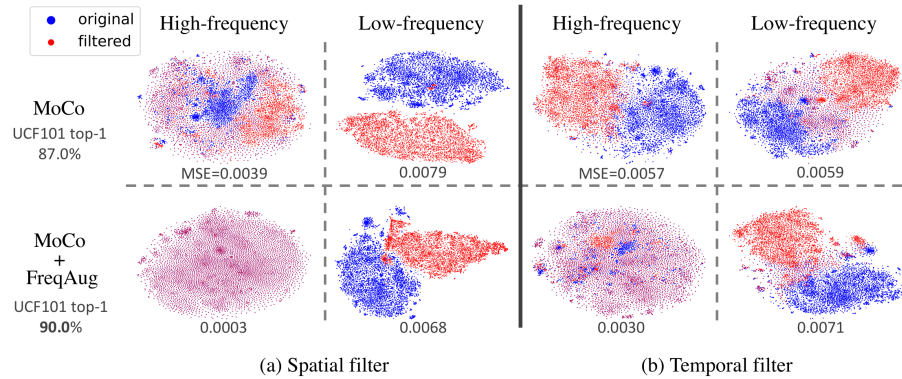


Fig. 4: **t-SNE visualization of the output features from original (blue) and frequency filtered (red) frames.** Mean squared error (MSE) between two features are presented under each plot. MoCo pretrained SlowOnly-50 models with or without FreqAug (and their UCF101 finetuning accuracies) are compared. FreqAug makes features of high-frequency components close to that of original clips which results in better downstream performance. If red and blue dots are too close, they can be perceived as purple.

observe that the distance between original clips and its spatial and temporal HFC substantially decreased when the model is pretrained with FreqAug while there are relatively small changes in the distance between the clip and its LFC; which means FreqAug does not reduce the overall distance between features. It indicates that FreqAug makes the model extract relatively more features from HFC via invariance learning between HFC and all frequency components in the original signal. The effect is more prominent in the temporal dimension probably because baseline augmentation already contains several spatial augmentations. We believe the feature representation learned via FreqAug whose HFC has been enhanced leads to better transferability of the model as empirically shown in Section 4. Please refer to the Appendix for more analysis on FreqAug.

## 6 Conclusion

In this paper, we have proposed a simple and effective frequency domain augmentation method for video representation learning. FreqAug augments multiple views by randomly removing spatial and temporal low-frequency components from videos so that a model can learn from the essential features. Extensive experiments have shown the effectiveness of FreqAug for various self-supervised learning frameworks and diverse backbones on *seven* downstream tasks. Especially, FreqAug enhances video SSL on relatively small data so that the downstream performance of the learned representation could close the gap to the models pretrained on the larger dataset. This opens up the possibility of learning video representation from domains with limited data.

## References

1. Alayrac, J.B., Recasens, A., Schneider, R., Arandjelović, R., Ramapuram, J., De Fauw, J., Smaira, L., Dieleman, S., Zisserman, A.: Self-supervised multimodal versatile networks. In: NeurIPS. pp. 25–37 (2020) [1](#), [3](#)
2. Alwassel, H., Mahajan, D., Korbar, B., Torresani, L., Ghanem, B., Tran, D.: Self-supervised learning by cross-modal audio-video clustering. In: NeurIPS (2020) [3](#)
3. Bai, Y., Yang, Y., Zhang, W., Mei, T.: Directional self-supervised learning for risky image augmentations. arXiv preprint arXiv:2110.13555 (2021) [9](#)
4. Behrmann, N., Fayyaz, M., Gall, J., Noroozi, M.: Long short view feature decomposition via contrastive video representation learning. In: ICCV. pp. 9244–9253 (October 2021) [7](#), [12](#), [13](#), [21](#)
5. Caron, M., Misra, I., Mairal, J., Goyal, P., Bojanowski, P., Joulin, A.: Unsupervised learning of visual features by contrasting cluster assignments. In: NeurIPS (2020) [1](#), [3](#), [4](#)
6. Carreira, J., Zisserman, A.: Quo vadis, action recognition? a new model and the kinetics dataset. In: CVPR. pp. 4724–4733 (2017) [7](#)
7. Chen, P., Huang, D., He, D., Long, X., Zeng, R., Wen, S., Tan, M., Gan, C.: Rspnet: Relative speed perception for unsupervised video representation learning. In: AAAI (2021) [1](#), [2](#), [3](#), [11](#)
8. Chen, T., Kornblith, S., Norouzi, M., Hinton, G.: A simple framework for contrastive learning of visual representations. In: ICML. pp. 1597–1607 (2020) [1](#), [3](#), [4](#), [8](#), [21](#)
9. Chen, X., Fan, H., Girshick, R.B., He, K.: Improved baselines with momentum contrastive learning. arXiv preprint arXiv:2003.04297 (2020) [3](#), [4](#), [7](#), [8](#), [19](#), [21](#)
10. Chen, X., He, K.: Exploring simple siamese representation learning. In: CVPR. pp. 15750–15758 (June 2021) [3](#), [8](#), [21](#)
11. Dave, I., Gupta, R., Rizve, M.N., Shah, M.: Tclr: Temporal contrastive learning for video representation. arXiv preprint arXiv:2101.07974 (2021) [2](#)
12. Devlin, J., Chang, M.W., Lee, K., Toutanova, K.: Bert: Pre-training of deep bidirectional transformers for language understanding. arXiv preprint arXiv:1810.04805 (2018) [1](#)
13. Fan, H., Li, Y., Xiong, B., Lo, W.Y., Feichtenhofer, C.: Pyslowfast. <https://github.com/facebookresearch/slowfast> (2020) [12](#)
14. Farha, Y.A., Gall, J.: MS-TCN: multi-stage temporal convolutional network for action segmentation. In: CVPR. pp. 3575–3584 (2019) [7](#), [12](#), [20](#), [21](#)
15. Feichtenhofer, C., Fan, H., Malik, J., He, K.: Slowfast networks for video recognition. In: ICCV (October 2019) [8](#), [20](#), [21](#)
16. Feichtenhofer, C., Fan, H., Xiong, B., Girshick, R., He, K.: A large-scale study on unsupervised spatiotemporal representation learning. In: CVPR. pp. 3299–3309 (June 2021) [1](#), [2](#), [4](#), [7](#), [11](#), [21](#), [23](#)
17. Goyal, R., Kahou, S.E., Michalski, V., Materzynska, J., Westphal, S., Kim, H., Haenel, V., Fründ, I., Yianilos, P., Mueller-Freitag, M., Hoppe, F., Thureau, C., Bax, I., Memisevic, R.: The “something something” video database for learning and evaluating visual common sense. In: ICCV. pp. 5843–5851 (2017) [3](#), [7](#), [20](#)
18. Grill, J.B., Strub, F., Altché, F., Tallec, C., Richemond, P., Buchatskaya, E., Dohersch, C., Avila Pires, B., Guo, Z., Gheshlaghi Azar, M., Piot, B., Kavukcuoglu, k., Munos, R., Valko, M.: Bootstrap your own latent - a new approach to self-supervised learning. In: NeurIPS. pp. 21271–21284 (2020) [1](#), [3](#), [4](#), [8](#), [21](#)

19. Han, T., Xie, W., Zisserman, A.: Self-supervised co-training for video representation learning. In: NeurIPS (2020) [1](#), [3](#)
20. Hara, K., Kataoka, H., Satoh, Y.: Can spatiotemporal 3d cnns retrace the history of 2d cnns and imagenet? In: CVPR. pp. 6546–6555 (2018) [8](#), [21](#)
21. He, K., Fan, H., Wu, Y., Xie, S., Girshick, R.: Momentum contrast for unsupervised visual representation learning. In: CVPR (2020) [1](#), [3](#), [6](#)
22. Huang, D., Wu, W., Hu, W., Liu, X., He, D., Wu, Z., Wu, X., Tan, M., Ding, E.: Ascnet: Self-supervised video representation learning with appearance-speed consistency. In: ICCV. pp. 8096–8105 (October 2021) [11](#)
23. Huang, L., Liu, Y., Wang, B., Pan, P., Xu, Y., Jin, R.: Self-supervised video representation learning by context and motion decoupling. In: CVPR. pp. 13886–13895 (2021) [1](#), [3](#)
24. Idrees, H., Zamir, A.R., Jiang, Y.G., Gorban, A., Laptev, I., Sukthankar, R., Shah, M.: The thumos challenge on action recognition for videos “in the wild”. *Computer Vision and Image Understanding* **155**, 1–23 (2017) [3](#), [7](#), [8](#), [13](#), [19](#), [20](#)
25. Ioffe, S., Szegedy, C.: Batch normalization: Accelerating deep network training by reducing internal covariate shift. In: ICML. pp. 448–456 (2015) [21](#)
26. Kim, G., Han, D.K., Ko, H.: Specmix : A mixed sample data augmentation method for training with time-frequency domain features. In: Proc. Interspeech (2021) [4](#)
27. Kim, J., Cha, S., Wee, D., Bae, S., Kim, J.: Regularization on spatio-temporally smoothed feature for action recognition. In: CVPR (June 2020) [3](#)
28. Kipf, T.N., Welling, M.: Semi-supervised classification with graph convolutional networks. In: ICLR (2017) [20](#)
29. Kuehne, H., Arslan, A.B., Serre, T.: The language of actions: Recovering the syntax and semantics of goal-directed human activities. In: CVPR (2014) [3](#), [7](#), [12](#), [19](#), [20](#)
30. Kuehne, H., Jhuang, H., Garrote, E., Poggio, T., Serre, T.: Hmdb: a large video database for human motion recognition. In: ICCV. pp. 2556–2563 (2011) [3](#), [7](#), [20](#)
31. Lee, K., Zhu, Y., Sohn, K., Li, C.L., Shin, J., Lee, H.: i-mix: A domain-agnostic strategy for contrastive representation learning. In: ICLR (2021) [29](#)
32. Li, Y., Li, Y., Vasconcelos, N.: Resound: Towards action recognition without representation bias. In: ECCV (2018) [2](#), [3](#), [7](#), [20](#)
33. Lin, J., Gan, C., Han, S.: Tsm: Temporal shift module for efficient video understanding. In: CVPR. pp. 7083–7093 (2019) [13](#)
34. Loshchilov, I., Hutter, F.: Sgdr: Stochastic gradient descent with warm restarts. In: ICLR (2017) [19](#)
35. van der Maaten, L., Hinton, G.: Visualizing data using t-sne. *Journal of Machine Learning Research* **9**(86), 2579–2605 (2008) [13](#)
36. Miech, A., Alayrac, J.B., Smaira, L., Laptev, I., Sivic, J., Zisserman, A.: End-to-End Learning of Visual Representations from Uncurated Instructional Videos. In: CVPR (2020) [3](#)
37. Nam, H., Kim, S.H., Park, Y.H.: Filteraugment: An acoustic environmental data augmentation method. arXiv preprint arXiv:2110.03282 (2021) [4](#)
38. Nam, J.H., Lee, S.C.: Frequency filtering for data augmentation in x-ray image classification. In: ICIP. pp. 81–85 (2021) [4](#)
39. Pan, T., Song, Y., Yang, T., Jiang, W., Liu, W.: Videomoco: Contrastive video representation learning with temporally adversarial examples. In: CVPR. pp. 11205–11214 (2021) [2](#)
40. Park, D.S., Chan, W., Zhang, Y., Chiu, C.C., Zoph, B., Cubuk, E.D., Le, Q.V.: SpecAugment: A Simple Data Augmentation Method for Automatic Speech Recognition. In: Proc. Interspeech. pp. 2613–2617 (2019) [4](#)

41. Park, N., Kim, S.: How do vision transformers work? In: ICLR (2022) [26](#)
42. Paszke, A., Gross, S., Massa, F., Lerer, A., Bradbury, J., Chanan, G., Killeen, T., Lin, Z., Gimelshein, N., Antiga, L., Desmaison, A., Kopf, A., Yang, E., DeVito, Z., Raison, M., Tejani, A., Chilamkurthy, S., Steiner, B., Fang, L., Bai, J., Chintala, S.: Pytorch: An imperative style, high-performance deep learning library. In: NeurIPS, pp. 8024–8035 (2019) [19](#), [22](#)
43. Qian, R., Meng, T., Gong, B., Yang, M.H., Wang, H., Belongie, S., Cui, Y.: Spatiotemporal contrastive video representation learning. In: CVPR. pp. 6964–6974 (June 2021) [1](#), [2](#), [3](#), [11](#)
44. Radford, A., Wu, J., Child, R., Luan, D., Amodei, D., Sutskever, I., et al.: Language models are unsupervised multitask learners. OpenAI blog **1**(8), 9 (2019) [1](#)
45. Recasens, A., Luc, P., Alayrac, J., Wang, L., Strub, F., Tallec, C., Malinowski, M., Patraucean, V., Alth  , F., Valko, M., Grill, J., van den Oord, A., Zisserman, A.: Broaden your views for self-supervised video learning. In: ICCV (2021) [1](#), [3](#)
46. Shao, D., Zhao, Y., Dai, B., Lin, D.: Finegym: A hierarchical video dataset for fine-grained action understanding. In: CVPR (2020) [3](#), [7](#), [20](#)
47. Soomro, K., Zamir, A.R., Shah, M.: Ucf101: A dataset of 101 human actions classes from videos in the wild. arXiv preprint arXiv:1212.0402 (2012) [3](#), [7](#), [20](#)
48. Tian, Y., Sun, C., Poole, B., Krishnan, D., Schmid, C., Isola, P.: What makes for good views for contrastive learning? In: NeurIPS. vol. 33, pp. 6827–6839 (2020) [2](#)
49. Tran, D., Wang, H., Torresani, L., Ray, J., LeCun, Y., Paluri, M.: A closer look at spatiotemporal convolutions for action recognition. In: IEEE Conference on Computer Vision and Pattern Recognition (CVPR). pp. 6450–6459 (2018) [8](#), [21](#)
50. Wang, H., Wu, X., Huang, Z., Xing, E.P.: High-frequency component helps explain the generalization of convolutional neural networks. In: CVPR (June 2020) [3](#)
51. Wang, J., Gao, Y., Li, K., Jiang, X., Guo, X., Ji, R., Sun, X.: Enhancing unsupervised video representation learning by decoupling the scene and the motion. In: AAAI (2021) [3](#)
52. Wang, J., Gao, Y., Li, K., Lin, Y., Ma, A.J., Cheng, H., Peng, P., Ji, R., Sun, X.: Removing the background by adding the background: Towards background robust self-supervised video representation learning. In: CVPR (2021) [1](#), [2](#), [4](#), [11](#), [29](#)
53. Wang, L., Xiong, Y., Wang, Z., Qiao, Y., Lin, D., Tang, X., Van Gool, L.: Temporal segment networks: Towards good practices for deep action recognition. In: ECCV. pp. 20–36 (2016) [13](#), [20](#)
54. Wen, Z., Li, Y.: Toward understanding the feature learning process of self-supervised contrastive learning. In: ICML. pp. 11112–11122 (2021) [1](#)
55. Wu, Z., Xiong, Y., Yu, S.X., Lin, D.: Unsupervised feature learning via non-parametric instance discrimination. In: CVPR. pp. 3733–3742 (2018) [3](#)
56. Xiao, F., Tighe, J., Modolo, D.: Modist: Motion distillation for self-supervised video representation learning. arXiv preprint arXiv:2106.09703 (2021) [1](#), [3](#)
57. Xie, S., Sun, C., Huang, J., Tu, Z., Murphy, K.: Rethinking spatiotemporal feature learning: Speed-accuracy trade-off in video classification. In: ECCV. pp. 318–335 (2018) [7](#), [8](#), [21](#)
58. Xu, M., P  rez-R  a, J.M., Escorcia, V., Martinez, B., Zhu, X., Zhang, L., Ghanem, B., Xiang, T.: Boundary-sensitive pre-training for temporal localization in videos. In: CVPR. pp. 7220–7230 (2021) [12](#), [13](#)
59. Xu, M., Zhao, C., Rojas, D.S., Thabet, A., Ghanem, B.: G-tad: Sub-graph localization for temporal action detection. In: CVPR. pp. 10156–10165 (2020) [8](#), [12](#), [13](#), [20](#), [21](#)
60. Xu, Q., Zhang, R., Zhang, Y., Wang, Y., Tian, Q.: A fourier-based framework for domain generalization. In: CVPR. pp. 14383–14392 (2021) [4](#)

- 61. Xu, Z., Liu, D., Yang, J., Raffel, C., Niethammer, M.: Robust and generalizable visual representation learning via random convolutions. In: ICLR (2021) [29](#)
- 62. Yang, Z., Dai, Z., Yang, Y., Carbonell, J., Salakhutdinov, R.R., Le, Q.V.: Xlnet: Generalized autoregressive pretraining for language understanding. NeurIPS **32** (2019) [1](#)
- 63. Zhao, N., Wu, Z., Lau, R.W., Lin, S.: What makes instance discrimination good for transfer learning? In: ICLR (2021) [2](#)



## Appendix

### A Datasets and Implementation Details

#### A.1 Localization Datasets

Breakfast [29] dataset contains 1,712 untrimmed videos with temporal annotations of 48 actions related to breakfast preparation. On average, 6 action instances are contained in each video. THUMOS'14 [24] is a dataset which consists of 413 untrimmed videos of 20 actions for temporal action localization task; there are 200 videos for the training and 213 videos for the evaluation.

#### A.2 Self-supervised Pretraining

For self-supervised pretraining, we use SGD with momentum of 0.9, half-cosine learning rate schedule [34], and linear warm-up for the first 35 epochs. By default, all the models are trained for 200 epochs. The base learning rate is set to 1.6 and 4.0 for MK200 and K400 experiment, respectively, and weight decay is set to  $1e-5$ . The linear warm-up starts from 0.001.

In terms of spatial augmentation, a combination of resizing, cropping, horizontal flipping, color jittering, Gaussian blurring, and random grayscaling is applied in a temporally consistent manner as our baseline following [9]. For random resized cropping, we randomly sample a sub-region with the scale between (0.2, 1.0) and the aspect ratio between (3/4, 4/3) of the original frame followed by scaling the size to  $224 \times 224$ . For color jittering, brightness, contrast, saturation, and hue are adjusted randomly with a probability of 0.8. Each attribute is modified by using `adjust_{attribute}` method in `torchvision.transforms.functional` module of Pytorch [42]. Each factor is uniformly sampled within a range of [0.6, 1.4] for the first three attributes, and a range of [-0.1, 0.1] for the last. Gaussian blurring is applied with the probability of 0.5 and the standard deviation sampled from  $Uniform(0.1, 2.0)$ . Frames are turned into grayscale with the probability of 0.2.

For temporal augmentation, randomly sampled clips from different timestamps compose the positive instances for learning temporally persistent representation. Also, we put a constraint on the temporal sampling that two clips should be sampled within a range of 1 second from each clip's center frame. Each clip consists of  $T$  frames sampled from  $T \times \tau$  consecutive frames with stride  $\tau$ . We apply the identical baseline augmentation strategy for all the SSL methods used in the main paper.

Recently, some deep learning libraries, *e.g.* Pytorch [42], offer a GPU accelerated version of fast Fourier transform (FFT) and inverse FFT (iFFT) functions, which are efficient implementations of DFT and iDFT. Thus we utilize these algorithms for FreqAug. We choose two default settings for FreqAug unless specified. FreqAug-T (temporal) uses temporal high-pass filter (HPF) with cutoff frequency 0.1 and probability 0.5. FreqAug-ST (spatio-temporal) is a combination of spatial HPF with cutoff frequency 0.01 alongside with FreqAug-T.

### A.3 Downstream Tasks

**Finetuning and low-shot learning.** For supervised finetuning and low-shot learning, we train the models for 200 epochs with a base learning rate of 0.025, zero weight decay, and without warm-up. Only basic spatial augmentations are used for finetuning and low-shot learning: random resizing (shorter side to [256, 320]), random cropping (224×224 pixels from resized frames), and random horizontal flipping. Random horizontal flipping is excluded in the case of SSv2 because the dataset has direction-sensitive action categories. For UCF101 [47] and HMDB51 [30], temporal augmentation draws  $T \times \tau$  consecutive frames randomly and uniformly sub-samples  $T$  frames for the input. For Diving48 [32], Gym99 [46], and Something-something-v2 (SSv2) [17], segment-based sampling [53] is applied, which divides a video into  $T$  equal length segments and samples one frame randomly from each segment. Dropout with the drop probability of 0.8 is applied before the linear classifier.

**Temporal Action Localizaton.** We evaluate the learned representation on two temporal action localization tasks: action segmentation that allocates every frame into pre-defined action class and action localization that localizes class-specific temporal action snippets from backgrounds. Both tasks aims at evaluating the ability of learned features to recognize temporal changes of action.

We train an action segmentation model, Multi-Stage Temporal Convolutional Network (MS-TCN) [14], on Breakfast dataset [29] with frozen features from the pretrained encoder. MS-TCN is composed of four stages with ten layers each. Each layer is a sequence of a 1D dilated convolution, ReLU activation, and a  $1 \times 1$  convolution, and has a residual connection. The features of videos in Breakfast dataset are extracted by the pretrained encoder with the sliding window fashion. The FPS of the videos are fixed to 15 and the size of the sliding window is  $21 \times 1$  (number of frames  $\times$  stride). Refer to [14] for other MS-TCN settings.

For temporal action localization task, we train Graph-Temporal Action Detection (G-TAD) [59] model on THUMOS'14 [24] dataset. G-TAD treats a video sequence as a graph and solves action detection as a sub-graph localization problem using a set of graph convolution network (GCN) [28] and a sub-graph of interest alignment layer. We extract video features with  $9 \times 1$  sliding window in the case of pretrained SlowOnly encoder; we use officially released feature<sup>4</sup> for TSN [53]. All other G-TAD related settings are set fixed as its original paper [59].

### A.4 Evaluation

We report top-1 accuracy as the performance measure for action recognition downstream tasks. For Kinetics, UCF101, and HMDB51, we report the averaged accuracy over 30-crops, *i.e.* temporally 10-crops and spatially 3-crops, following standard practices [15]. All frames are resized to fit its shorter side to 256 and uniformly samples three 256×256 crops along the other axis. Similarly, ten clips, equally distributed in the temporal axis, are sampled for each spatial crop.

<sup>4</sup> <https://github.com/frostinassiky/gtad>

For Diving48, Gym99, and SSv2, we report spatially 3-crop accuracy with the segment-based temporal sampling. Note that  $\tau$  can be ignored for the datasets with the segment-based sampling strategy.

Following [14], the evaluation metrics for temporal action segmentation task are the frame-wise accuracy, the edit distance, and the F1 scores at the overlapping threshold of 10%, 25%, and 50%. The temporal intersection over union (IoU) is used to measure the overlap between the predicted action and the ground truth for the F1 score. The models are evaluated on the split-1 of Breakfast dataset, following the previous work [4]. For a better reliability, we report average scores of 10 evaluations with different random seeds.

For temporal action localization, we measure mean average precision (mAP) at IoU threshold from 0.3 to 0.7 with stride 0.1 following [59]. We also report average mAP over the 5 IoU thresholds. All metrics are averaged over 5 different runs for a better reliability.

## A.5 Models

**Backbone.** Our default encoder backbone is SlowOnly-50 which is a variant of 3D Residual Network (ResNet) originated from the slow branch of SlowFast network [15]. It shows decent action recognition performances with affordable computations compared to other variants thanks to its architectural choices, *e.g.*, decomposed spatial and temporal convolutions, no temporal downsampling, large temporal stride ( $\tau$ ), and temporal convolutions only at the last two stages. We also evaluate our method on 3D-ResNet-18 (R-18) [20], R(2+1)D [49] and S3D-G [57] models. R-18 is a 3D-ResNet with full 3D convolutions and R(2+1)D is another popular variant of 3D ResNet with factorized 3D convolution filter. S3D-G is an inception-style 3D model with gating modules.

**SSL Methods.** We implement MoCo [9], BYOL [18], and SimSiam [10] with some hyperparameter changes for the video model. For MoCo, the projection MLP has one hidden layer with 2048 hidden and 128 output dimensions. The size of queue and temperature for infoNCE loss are set to 65536 and 0.1, respectively. We additionally use cosine annealing of the momentum coefficient from 0.994 to 1.0 following [16]. The batch size of MoCo is 128 and 256 for MK200 and K400 experiments, respectively. For BYOL, the projection MLP has one hidden layer with 4096 hidden and 256 output dimensions. The prediction MLP has the identical structure to the projection head. The decay rate for the target encoder is annealed from 0.99 to 1.0 with a cosine schedule. For SimSiam, the projection MLP has 2 hidden layers with 2048 hidden and 128 output dimensions. The prediction MLP has one bottleneck type hidden layer with dimension of 512. All the MLP hidden layers for MoCo, BYOL, and SimSiam are equipped with a batch normalization (BN) [25] and a ReLU activation. The projection MLP of SimSiam has a BN after output linear layer. For both BYOL and SimSiam, batch size of 64 is set and the synchronized BN [8] is used in the model.

## B Pseudo-code

---

**Algorithm 1** FreqAug: Pytorch-like Pseudocode

---

```

# x: video, B X C X T X H X W
# p: filter probability
# co_s, co_t: spatial and temporal cutoff freq.
# type_s, type_t: HPF if True else LPF
# fftfreq: calculate FFT sample frequencies
# outer: outer product

def freqaug(x, p, co_s, co_t, type_s, type_t):
    if random() < p: # U(0,1)
        # pass bands
        pass_t = torch.abs(torch.fft.fftfreq(T)) < co_t
        pass_h = torch.abs(torch.fft.fftfreq(H)) < co_s
        pass_w = torch.abs(torch.fft.fftfreq(W)) < co_s

        pass_hw = torch.outer(pass_h, pass_w)
        if type_s:
            pass_hw = torch.logical_not(pass_hw)

        if type_t:
            pass_t = torch.logical_not(pass_t)

        F = torch.outer(pass_t, pass_hw.view(-1)).view(T, H, W) # filter
        X = torch.fft.fft(x) # FFT, X: spectrum
        X_hat = F * X # filtering
        return torch.fft.ifft(X_hat) # inverse FFT
    else:
        return x

```

---

We provide a Python-style pseudo-code of FreqAug with PyTorch [42] package in Algorithm 1. As shown in the code, FreqAug can be implemented with only a few lines. In the case when the augmentation is applied (`random() < p`), the filter ( $F$ ) is constructed according to the cutoff frequencies (`co_s`, `co_t`) at first, then 1) transforming the input ( $x$ ) to the spectrum ( $X$ ) by FFT, 2) applying the filter by element-wise multiplication and 3) transforming the filtered spectrum ( $X_{\text{hat}}$ ) back to the original domain by iFFT are sequentially applied.

Since our method is a data augmentation applied before the video sample is fed to the encoder, the attached code is easily integrated into general PyTorch-based video SSL implementations.

## C Additional Results

### C.1 Additional Evaluations

In Table 7, we report three additional evaluation results of MK200-pretrained SlowOnly-50 (SO-50) in the MoCo framework: 1) linear evaluation on the pre-

Table 7: **Additional evaluations of MoCo with FreqAug.** Results of linear evaluation on the pretrained dataset (MK200) and finetuning (Not low-shot) on relatively large datasets (Gym99 and SSv2) are presented. Three augmentation probabilities for FreqAug-T and FreqAug-ST are evaluated. All backbones are SO-50.

Method	FreqAug prob.	Linear	Finetuning	
		MK200	Gym99	SSv2
Baseline	-	65.3	88.2	57.2
FreqAug-T	0.1	66.6	89.1	58.0
FreqAug-T	0.3	67.2	89.5	<b>58.4</b>
FreqAug-T	0.5	<b>67.4</b>	89.3	58.2
FreqAug-ST	0.1	<b>67.4</b>	88.8	57.8
FreqAug-ST	0.3	66.9	89.1	58.1
FreqAug-ST	0.5	67.3	<b>89.6</b>	<b>58.4</b>

trained dataset (MK200); 2) finetuning on Gym99; 3) finetuning on SSv2. Note that all the pretrained models are the same models presented in the main paper.

**Linear evaluation.** Linear evaluation protocol which trains a linear classifier on top of a frozen encoder, is often applied on the pretrained dataset for evaluating the learned representation by video SSL [16]. The linear classifier is trained for 60 epochs with the cosine learning rate schedule, zero weight decay, and the linear warm-up. The base learning rate for the schedule is set to 0.5. The warm-up starts from 0.001 and lasts for the first 8 epochs. The data augmentations during training and evaluation protocols are the same as the finetuning setting on UCF101 and HMDB51.

Similar to other downstream tasks, MoCo with FreqAug surpasses the baseline for all the augmentation probabilities ( $p$ ), which implies the learned representations get more discriminative with FreqAug.

**Finetuning on Gym99 and SSv2.** The finetuning setting used for Gym99 is identical to that of other datasets in the main paper. Since SSv2 is a relatively large dataset, we follow the training recipe in the previous work [16]. The models are finetuned for 22 epochs with the initial learning rate of 0.06, weight decay of  $1e-6$ , and batch size of 64. We use the step-wise learning rate decay at 14 and 18 epoch by  $1/10$ . We set the dropout probability of 0.5.

We observe again that FreqAug improves the performance over the baseline regardless of the augmentation probability. The trend, that FreqAug with higher  $p$  usually shows better accuracy, is similar to the low-shot learning in the main paper. However, the difference between them is less clear than the low-shot learning results presumably because of the relatively large dataset size of the downstream task as we claimed in the main paper.

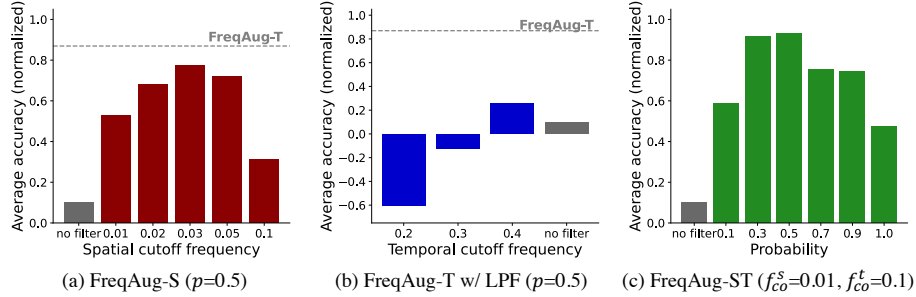


Fig. 5: **Additional FreqAug hyperparameter ablations on Mini-Kinetics.** Three parameters are searched: (a) spatial cutoff frequency for FreqAug-S and (b) temporal cutoff frequency for FreqAug-T with low-pass filter (LPF) and (c) augmentation probability for FreqAug-ST. Other parameters is set fixed as in the parenthesis. MoCo-pretrained SlowOnly-50 are used as a backbone. Min-max normalized accuracies of 5 tasks are averaged; min/max values calculated for Fig. 3 in the main paper are used for better comparison.

## C.2 Additional Ablation Studies on Hyperparameters

In addition to Sec. 4.3, we conduct additional ablation studies on FreqAug hyperparameters in Fig. 5. Note that we use the same min/max values for Fig. 3 in the main paper for the normalization. Therefore, some scores can be below zero if one model’s accuracy is lower than the lowest accuracy of the models in Fig. 3.

First, we examine spatial-filter-only variants of FreqAug (FreqAug-S) in Fig. 5 (a) by testing several  $f_{co}^s$ . We observe that FreqAug-S also outperforms the baseline, but it is worse than the default FreqAug-T. Second, accuracies of low-pass filter (LPF) counterpart of FreqAug-T with different  $f_{co}^t$  are displayed in Fig. 5 (b). The accuracy becomes less than the baseline as  $f_{co}^t$  gets smaller, *i.e.* as more high-frequency components are removed. The results clearly demonstrate that the performance improvement via FreqAug with HPF is not just due to the randomness and each frequency component has a different influence on the downstream performance. Lastly,  $p$  of FreqAug-ST is searched in a range of  $[0.0, 1.0]$  while keeping  $f_{co}^s$  and  $f_{co}^t$  fixed in Fig. 5 (c). We found that the trend is similar to the case of FreqAug-T in Fig. 3(b) of the main paper; the overall downstream performance is the best when  $p = 0.5$ .

## C.3 Ablation Studies on Views

In the main paper, we applied FreqAug to both views of the video SSL models as the default setting. On the other hands, we individually apply FreqAug-T to single view of MoCo in Table 8. View-1 and view-2 indicate the inputs for the trainable encoder and the momentum encoder, respectively. We observe that our default setting is generally better on the five action recognition downstream tasks

Table 8: **Impact of FreqAug only on a single view.** FreqAug column indicates the views which FreqAug is applied and the augmentation probability for FreqAug. View-2 is input for the momentum encoder. Tested with MoCo and FreqAug-T on MK200. All backbones are SlowOnly-50.

FreqAug			Finetune			Low-shot	
view 1	view 2	$p$	UCF101	HMDB51	Diving48	Gym99-10%	SSv2-10%
			87.0	56.5	67.8	29.9	25.3
✓		0.5	88.8	56.7	<b>71.4</b>	30.4	25.7
✓		1.0	86.8	54.6	68.3	30.2	24.6
	✓	0.5	88.9	59.9	66.5	<b>35.7</b>	27.4
	✓	1.0	86.9	57.8	65.9	33.4	26.2
✓	✓	0.5	<b>89.8</b>	<b>60.8</b>	70.3	35.2	<b>28.1</b>

than the single view counterparts. Compared to the default setting, FreqAug-T on view-1 shows higher top-1 accuracy on Diving48 but significantly worse performance on the others. FreqAug-T on view-2 shows a marginal improvement on Gym99 dataset but a considerable degradation on Diving 48. FreqAug-T on both views achieves decent performance without a significant loss on any task. We also provide results of single-view FreqAug with  $p = 1.0$  where one of the views is always filtered. In this case, the invariance between two views with all frequency components cannot be learned. The reduced performances of the case  $p = 1.0$  support our claim that invariance learning between different frequency components needs to be properly adjusted by  $p$ , rather than learning from *only* low- or high-frequency components. Further analysis on the impact of applying FreqAug to each stream on each downstream task remains for future research.

#### C.4 Qualitative Results of Action Segmentation

The qualitative results of the temporal action segmentation task are presented in Fig. 6. Two features pretrained by MoCo with the baseline augmentation (Base) and +FreqAug-T (FreqAug) can be compared with the ground-truth (GT) label. The quality of the segmentation with FreqAug is much better than the baseline; the classification and the boundaries of actions are more precise. As discussed in the main paper, we observe that the background scene in the Breakfast dataset rarely changes, so it makes the learned representation with FreqAug more effective on this task.

## D Additional Discussions

### D.1 Analysis on Static Video

In addition to Sec. 5.2 in the main paper, we also visualize the distance between the model’s output feature of the original videos and that of the static videos





Fig. 6: **Qualitative results of temporal action segmentation on the Breakfast dataset.** Bar plot displays predictions of pretrained features with the baseline augmentation (Base) and FreqAug-T (FreqAug) along with the ground-truth (GT). SlowOnly-50 encoders are pretrained by MoCo framework and MS-TCN is trained on top of frozen features from the pretrained encoder.

in Fig. 7. Here, a static video indicates a synthesized video with duplicated center frames thus there is no temporal information; it may or may not have important spatial features depending on the frame. We compare three features from MoCo-pretrained SlowOnly-50 on MK200: the baseline, with FreqAug-ST, and with FreqAug-T. We use mean squared error (MSE) as the distance metric, and use videos in the validation set of MK200 for the visualization. We observed that the two feature distributions are much closer for the MoCo baseline than for the models trained with FreqAug. It implies that the baseline model extracts more spatial features from the original video since static videos have only spatial cues. On the other hand, FreqAug makes the two distributions apart. It means the models trained with FreqAug extract fewer features from static videos which have non-zero components only at where the temporal frequency is zero. We believe that the feature representation of the model trained with FreqAug whose temporal zero-frequency components have been weakened can affect the downstream performance of the model.

## D.2 Analysis on Frequency Amplitude in the Feature Map

For analyzing the effect of FreqAug on the feature, we choose a method that visualizes the relative log amplitude of frequency components of the feature map in Fig. 8. The method is originally proposed to compare convolution and self-attention operations in [41]. The feature map for each layer is displayed in

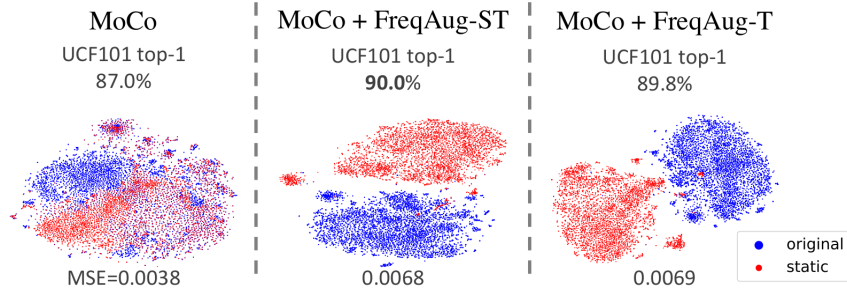


Fig. 7: **t-SNE visualization of the output features from the original (blue) and static (red) video.** A static video is a synthesized video with repetitions of the center frame without any temporal change. Mean squared error (MSE) between two features is presented under each plot. MoCo pretrained SlowOnly-50 models with or without FreqAug (and their UCF101 finetuning accuracies) are compared. FreqAug makes features of the static videos far from that of original videos which results in better downstream performance. When red and blue dots are too close, they can be perceived as purple.

different colors according to the depth of the layer. The depth is normalized for visualization, so 0.0 indicates the first layer and 1.0 indicates the last layer. The vertical axis of the graph represents the log amplitude at each frequency relative to the log amplitude at the zero frequency by substituting it. The horizontal axis denotes normalized frequency along the spatial or temporal axis. Two models, MoCo pretrained SO-50 with and without FreqAug-T, are compared. First, we found that relative amplitude for MoCo baseline model shows different trends in spatial and temporal frequency. In the spatial axis, relative frequency amplitudes get larger as the signal goes through the stages (a set of layers) while the amplitudes are rather mixed in the temporal axis. Second, when FreqAug-T is added, high-frequency (larger than zero) amplitudes of some intermediate layers become increased especially in the temporal axis. We believe that FreqAug-T affects the temporal frequency of the middle layers because only later stages of SO-50 contain temporal convolutions for the temporal modeling. This analysis supports our claim that FreqAug makes the model exploit relatively more high-frequency components by showing a relative increase of high-frequency amplitudes in intermediate feature maps.

### D.3 Comparison with Spatio-temporal Filter

One may wonder the reason for filtering in the frequency domain rather than in the spatio-temporal domain. For example, Gaussian blurring, *i.e.* convolution of Gaussian kernel, is a simple low-pass filter (LPF) in the spatio-temporal domain. First, designing filters in the frequency domain is more intuitive, especially for multi-dimensional signals, since the desired frequency band can be chosen sim-

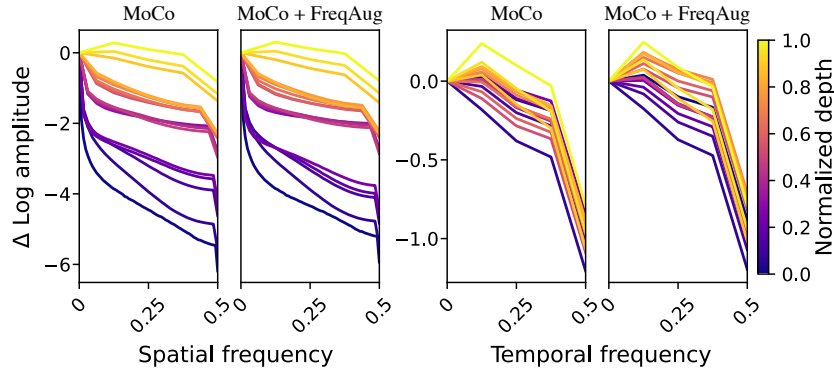


Fig. 8: **Relative log amplitude of frequency components in feature maps: spatial (left) and temporal (right) axis.** Color represents the normalized depth of each layer (lower value means closer to the input).  $\Delta$  Log amplitude is the difference between the log amplitude at each frequency and at zero-frequency (0.0). Features from MoCo-pretrained SlowOnly-50 encoders are visualized. MoCo with FreqAug-T increases the relative amplitude, especially for temporal frequency components, in some intermediate layers.

Table 9: **Comparison with other methods:** (a) Gaussian filters (GF) with different kernel sizes ( $k$ ) and std. ( $\sigma$ ) in spatio-temporal domain and (b) other augmentations. All methods are tested with MoCo-pretrained SlowOnly-50 on MK200.

	Method	Finetune			Low-shot	
		UCF101	HMDB51	Diving48	Gym99-10%	SSv2-10%
(a)	Baseline	87.0	56.5	67.8	29.9	25.3
	FreqAug-ST	<b>90.0</b>	<b>61.6</b>	<b>71.0</b>	<b>34.8</b>	28.1
	GF ( $k=3$ , $\sigma=0.5$ )	88.7	56.9	69.7	33.4	27.0
	GF ( $k=3$ , $\sigma=2.0$ )	88.3	58.4	68.9	33.4	26.0
	GF ( $k=7$ , $\sigma=0.5$ )	88.9	58.7	68.3	31.7	27.4
	GF2D ( $k=3$ , $\sigma=0.5$ )	87.0	58.2	67.1	31.5	<b>28.9</b>
	GF2D ( $k=3$ , $\sigma=2.0$ )	86.9	58.6	66.3	31.9	27.4
	GF2D ( $k=7$ , $\sigma=0.5$ )	87.6	59.2	68.4	32.4	28.1
(b)	RandConv	88.4	61.5	67.0	34.5	28.4
	RandConv3D	87.2	57.8	69.0	32.3	26.8
	Mixup (InputMix)	85.8	54.4	69.0	31.9	24.2
	Frame Mixup (BE)	88.8	57.5	68.2	30.8	25.4

ply by multiplying a filter mask. We also empirically test 3D Gaussian HPF (GF) with a few kernel sizes ( $k$ ) and standard deviations ( $\sigma$ ) in Table 9 (a). GF2D is a variant of GF with a spatial-only kernel. Both GF and GF2D mostly

show improvements over the baseline but not as much as FreqAug. In terms of training time, MoCo+FreqAug is around 10% faster than MoCo+GF( $k=3$ ) on 4 NVIDIA P40 GPUs (880, 981 sec/epoch on MK200 respectively). These imply that filtering in the frequency domain may also have advantages in terms of computational performance depending on the type of the spatio-temporal filter.

#### D.4 Comparison with Other Augmentation Methods

We compare FreqAug with several other regularization methods: RandConv ( $\text{RC}_{\text{img}1-7, p=0.5}$  in [61]), Mixup (InputMix in [31]) and static frame Mixup (BE [52]) in Table 9 (b). According to Fig. 1 in [61], it seems that RandConv modulates the input signal while preserving some high-frequency components. RandConv3D is a direct extension of 2D kernels into 3D kernels with the same hyperparameters. Note that we only apply the augmentation on the input video and we do not apply any changes in the model or the loss for the fair comparison. RandConv and BE mostly improve the performance over the baseline while InputMix affects adversely. Previous work (Tab. 4 in [52]) also shows that naive Mixup is not helpful for the downstream performance. In conclusion, FreqAug generally outperforms the other methods.

#### D.5 Comparison with Optical Flow

Both optical flow and our method extract temporally changing patterns from the visual signal. Though optical flow is a powerful motion feature, using it in SSL is somewhat cumbersome. Aside from the cost to extract optical flow from the video, a dedicated encoder is usually required for processing it. If one wants to utilize optical flow as an additional branch, it will result in increased computation. Or, to replace a few RGB branches into optical flow branches is not always straightforward in some SSL methods. On the other hand, FreqAug can be seamlessly integrated into any RGB-based SSL method.

### E Visualizations

#### E.1 More Examples of Temporal Filtering

In Fig. 9, we present more visualization of temporal HPF with different number of input frames ( $T$ ), input stride ( $\tau$ ), and temporal cutoff frequencies ( $f_{co}^t$ ): (a)  $T \times \tau = 8 \times 8$ ,  $f_{co}^t = 0.1$  (default), (b)  $T \times \tau = 8 \times 8$ ,  $f_{co}^t = 0.2$ , and (c)  $T \times \tau = 16 \times 4$ ,  $f_{co}^t = 0.1$ . Three rows of each sample display original frames, filtered frames, and filtered spectrum in order. In the spectrum, the red box indicates the temporal frequencies which are filtered out. Temporal HPF with default setting (a) shows that static parts of the frames are attenuated, similar to the examples in the main paper. When  $f_{co}^t$  becomes larger (b), more portions of the spectrum are filtered out, and accordingly, more visual information is removed. As we found in Fig. 3(a) in the main paper, removing too much visual

information might cause inferior results. In (c), more frequency components are masked, though  $f_{co}^t$  is not changed, since frequencies are more densely sampled as  $T$  gets larger. This can result in a more attenuated signal in the spatio-temporal domain.

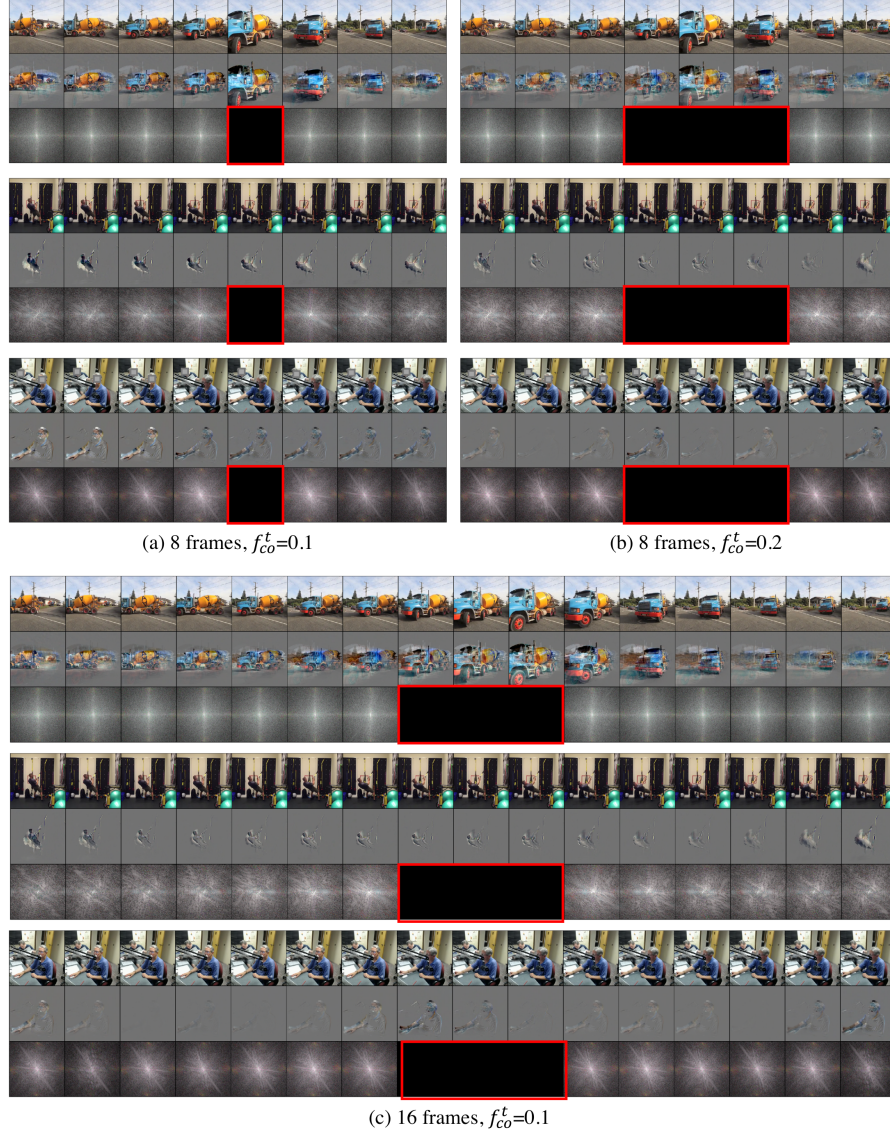


Fig. 9: **More examples of filtered frames and spectrum.** Three different settings (number of frames ( $T$ ) and temporal cutoff frequency ( $f_{co}^t$ )) for temporal high-pass filter (HPF) are displayed: (a)  $T = 8$ ,  $f_{co}^t = 0.1$  (default), (b)  $T = 8$ ,  $f_{co}^t = 0.2$ , and (c)  $T = 16$ ,  $f_{co}^t = 0.1$ . Top, middle, and bottom rows of each sample denote original frames, filtered frames, and filtered spectrum, respectively. In the spectrum, the red box indicates where the temporal frequency is filtered.